Title

Engineering A11 Minibody-Conjugated, Polypeptide-Based Gold Nanoshells for Prostate Stem Cell Antigen (PSCA)—Targeted Photothermal Therapy

Journal

SLAS TECHNOLOGY, 22(1)

ISSN

2472-6303

Authors

Mayle, Kristine M
Dern, Kathryn R
Wong, Vincent K
et al.

Publication Date

2017-02-01

DOI

10.1177/2211068216669710

Peer reviewed

Journal of
Laboratory Automation

Engineering A11 minibody-conjugated, polypeptide-based gold nanoshells for prostate stem cell antigen (PSCA)-targeted photothermal therapy

Journal:	*Journal of Laboratory Automation*
Manuscript ID	Draft
Manuscript Type:	Original Report
Date Submitted by the Author:	n/a
Complete List of Authors:	Mayle, Kristine Dern, Kathryn Wong, Vincent Chen, Kevin; UCLA, Bioengineering Sung, Shijun Ding, Ke Rodriguez, April Knowles, Scott; UCLA Taylor, Zachary Zhou, Z. Hong Grundfest, Warren Wu, Anna Deming, Timothy Kamei, Daniel; UCLA, Bioengineering
Keywords:	polypeptide vesicles, photothermal therapy, gold nanoshells
Abstract:	Currently, there is no curative treatment for advanced metastatic prostate cancer, and options, such as chemotherapy, are often nonspecific, harming healthy cells and resulting in severe side effects. Attaching targeting ligands to agents used in anti-cancer therapies has been shown to improve efficacy and reduce nonspecific toxicity. Furthermore, the use of triggered therapies can enable spatial and temporal control over the treatment. Here, we combined an engineered prostate cancer-specific targeting ligand, the A11 minibody, with a novel photothermal therapy agent, polypeptide-based gold nanoshells, which generate heat in response to near infrared light. We show that the A11 minibody strongly binds to the prostate stem cell antigen that is overexpressed on the surface of metastatic prostate cancer cells. Compared to non-conjugated gold nanoshells, our A11 minibody-conjugated gold nanoshell exhibited significant laser-induced, localized killing of prostate cancer cells in vitro. In addition, we improved upon a comprehensive heat transfer mathematical model that was previously developed by our laboratory. By relaxing some of the assumptions of our earlier model, we were able to generate more accurate predictions. Our experimental and theoretical results demonstrate the potential of our novel minibody-conjugated gold nanoshells for metastatic prostate cancer therapy.

Engineering A11 minibody-conjugated, polypeptide-based gold nanoshells for prostate stem cell antigen (PSCA)-targeted photothermal therapy

Kristine M. Mayle,[1] Kathryn R. Dern,[1] Vincent K. Wong,[1] Kevin Y. Chen[1], Shijun Sung,[2] Ke Ding,[1] April R. Rodriguez,[1] Scott Knowles[3], Zachary Taylor,[1,4] Z. Hong Zhou,[1,5,6] Warren S Grundfest,[1,2,4] Anna M. Wu,[3] Timothy J Deming,[1] and Daniel T Kamei[1,]*

[1]Department of Bioengineering, University of California, Los Angeles, CA 90095
[2]Department of Electrical Engineering, University of California, Los Angeles, CA 90095
[3]Department of Molecular and Medical Pharmacology, University of California, Los Angeles CA 90095
[4]Department of Surgery, University of California, Los Angeles, CA 90095
[5]Department of Microbiology, Immunology & Molecular Genetics, University of California, Los Angeles, CA 90095
[6]California NanoSystems Institute, University of California, Los Angeles, CA 90095

*Corresponding Author: Prof. Daniel T. Kamei, kamei@seas.ucla.edu

Keywords: polypeptide vesicles; photothermal therapy; gold nanoshells

Abstract

Currently, there is no curative treatment for advanced metastatic prostate cancer, and options, such as chemotherapy, are often nonspecific, harming healthy cells and resulting in severe side effects. Attaching targeting ligands to agents used in anti-cancer therapies has been shown to improve efficacy and reduce nonspecific toxicity. Furthermore, the use of triggered therapies can enable spatial and temporal control over the treatment. Here, we combined an engineered prostate cancer-specific targeting ligand, the A11 minibody, with a novel photothermal therapy agent, polypeptide-based gold nanoshells, which generate heat in response to near infrared light. We show that the A11 minibody strongly binds to the prostate stem cell antigen that is overexpressed on the surface of metastatic prostate cancer cells. Compared to non-conjugated gold nanoshells, our A11 minibody-conjugated gold nanoshell exhibited significant laser-induced, localized killing of prostate cancer cells *in vitro*. In addition, we improved upon a comprehensive heat transfer mathematical model that was previously developed by our laboratory. By relaxing some of the assumptions of our earlier model, we were able to generate more accurate predictions. Our experimental and theoretical results demonstrate the potential of our novel minibody-conjugated gold nanoshells for metastatic prostate cancer therapy.

1. Introduction

Prostate cancer cells can be targeted through prostate-specific membrane-bound antigens, such as prostate specific membrane antigen (PSMA) and prostate stem cell antigen (PSCA). In this research, we focused on targeting PSCA, which is predominantly prostate-specific and is overexpressed on prostate cancer cells with restrictive expression in normal tissues. PSCA

expression increases markedly with tumor stage, grade, and progression to androgen independence, where PSCA was found in 80% of localized tumors and all bone metastases[1,2]. The expression patterns of PSCA enable targeting of difficult-to-treat metastatic and androgen-independent tumor cells. Based on the promise of PSCA, researchers developed antibodies against PSCA, which could enable specificity in the treatment and imaging of prostate cancer.

One such targeting agent is the A11 minibody, which was developed for the purpose of detecting prostate cancer tumors using positron emission tomography (PET)[3]. The A11 minibody has enabled successful imaging of localized and metastatic prostate cancer with high contrast[3-5]. Its high affinity and specificity for PSCA-expressing cells also makes A11 an ideal candidate for targeting therapeutics to prostate cancer. Unlike many common cancer-targeting ligands, such as transferrin, A11 is not readily endocytosed by cells, but instead remains on the cell surface after binding with the antigen[5]. In order to exploit this strong binding, but low internalization properties of A11, we developed a targeted photothermal therapy agent, which can exert its cytotoxic effect while bound to the surface of cells.

In photothermal therapy, the energy from electromagnetic radiation is harnessed and converted into thermal energy to ablate tumor cells. Gold nanostructures have been investigated due to their ability to demonstrate surface plasmon resonance (SPR), where the conduction band electrons of the gold particles undergo coherent oscillation upon light irradiation[6]. At the peak SPR wavelength, the absorption of energy is significantly enhanced, which is important for the conversion of light into heat as the oscillation energy dissipates. In addition to using gold-based nanostructures for photothermal therapy, other laboratories have demonstrated the coupling of photothermal-capable gold nanostructures with gene expression profiling in cells[7,8]. The gold nanoshell structure, which consists of a thin layer of gold coated onto a dielectric core, has been

shown to demonstrate strong SPR in the near infrared region[9]. Near infrared-responsive agents are desired for a minimally invasive treatment, as near infrared light can best penetrate into tissue due to the low absorption coefficient of biological molecules, such as water and hemoglobin, and reduced scattering as compared to light in the visible region[9]. Furthermore, by using photothermal therapy together with the slow internalization rate of the A11 minibody, several advantages can be utilized compared to the photothermal effect induced by a gold nanoshell that exhibits significant internalization. First, the membrane disruption caused by thermal energy provides the most direct opportunity to damage the cell. In addition, the accumulation of gold nanoshells on the surface of the cell further focuses the photothermal effect into a confined area. Furthermore, the cell membrane has a relatively low thermal conductivity which can cause larger temperature gradients and subsequently more intense hyperthermic effects[10].

In this study, polypeptide vesicles are used as the core material of our gold nanoshells. As an emerging class of biomaterials, polypeptide vesicles have many benefits. Due to the wide variety of naturally occurring and synthetic amino acid building blocks, polypeptides can be engineered to exhibit unique chemical and physical properties. Additionally, polypeptide materials have the potential to exhibit low immunogenicity and toxicity. Polypeptide vesicles have also demonstrated the ability to encapsulate and deliver cargo, such as nucleic acids and anti-cancer drugs[11–13]. Moreover, the thicker vesicle bilayer, relative to conventional liposomes, increases the stability of the polypeptide vesicles due to greater attractive interactions between the long polypeptide chains.

In order to create the polypeptide-based gold nanoshells, we chemically deposited a thin layer of gold onto the polypeptide vesicle surface comprised of poly(L-lysine)$_{60}$-*block*-poly(L-leucine)$_{20}$ block copolypeptides ($K_{60}L_{20}$). The $K_{60}L_{20}$ vesicles were an ideal candidate for use as

a core material, since the abundance of amines present on the lysine blocks of the vesicle surface can form dative bonds with the gold to create an adherent shell. In this investigation, we aimed to use the A11 minibody to improve the specificity of the $K_{60}L_{20}$ gold nanoshells toward prostate cancer cells to enhance the efficacy of the photothermal therapy agent.

2. Materials and Methods

Synthesis of A11 Minibody

The A11 minibody was produced and purified as described previously by Wu and coworkers[4]. Briefly, the A11 scFv gene was fused to the human IgG1 hinge and C_H3 region downstream as well as to a signal peptide upstream, and inserted into the pEE12 expression vector. 10 µg of linearized plasmid DNA containing the minibody construct were used to transfect NS0 mouse myeloma cells by electroporation; selection was conducted in glutamine-deficient media; and a stable, high-producing subclone was isolated and expanded. Cell culture supernatants were conditioned using Dowex AG1x8 (Bio-Rad Laboratories, Irvine, CA) and the A11 minibody was purified by sequential chromatography on Capto MMC (GE Healthcare Life Science, Marlborough, MA), anion exchange using UNOsphere Q (Bio-Rad) and finally with CHT ceramic hydroxyapatite (Bio-Rad) as described[4]. After purification, the proteins were dialyzed against phosphate-buffered saline (PBS) and then concentrated with Vivaspin 20 centrifugal concentrators (MWCO: 30,000). UV absorbance at 280 nm was then measured to determine the final protein concentrations.

Radiolabeling the A11 Minibody

Tyrosine residues of A11 were radiolabeled with $Na^{125}I$ using IODO-BEADS (Pierce, Rockford, IL). Radiolabeled A11 samples were purified from free ^{125}I with a Sephadex G10 size-exclusion column with bovine serum albumin (BSA) added to prevent nonspecific binding to the column. The phosphotungstic acid (PTA) assay was used to quantify the specific activity and concentration of each radiolabeled sample[14].

Cellular Binding and Trafficking

PSCA-transfected 22Rv1 prostate cancer cells were seeded onto 35 mm dishes (Becton Dickinson and Company, Franklin Lakes, NJ) with a seeding density of 1.25×10^5 cells/cm^2 in growth medium. The growth medium was RPMI 1640 supplemented with 10% fetal bovine serum and 1% penicillin/streptomycin (pH 7.4). After 15 h of incubation in a humidified 5% CO_2 and 37°C environment, the growth medium was aspirated, and new incubation medium with 1 nM radiolabeled A11 was added to each dish. The incubation medium was RPMI 1640 supplemented with 20 mM 4-(2-hydroxyethyl)-1-piperazineethanesulfonic acid (HEPES) and 1% penicillin/streptomycin (pH 7.4). The cells were incubated in this medium at 37°C for 1, 2, 5, 7, 10, and 60 min. At each time point, the incubation medium was removed, and the cells were washed 5 times with ice-cold WHIPS (20 mM HEPES, 1 mg/mL polyvinylpyrrolidone (PVP), 130 mM NaCl, 5 mM KCl, 0.5 mM $MgCl_2$, and 1 mM $CaCl_2$, pH 7.4) to remove nonspecifically bound A11 on the cell surfaces. Cell-surface bound A11 was then separated from internalized A11 by adding 1 mL of ice-cold acid strip (50 mM glycine-HCl, 100 mM NaCl, 1 mg/mL PVP, and 2 M urea, pH 3.0) to each dish. The cells were placed on ice for 12 min. Each dish was then washed once more with 1 mL of acid strip. The radioactivity in the collected acid strip washes was quantified using a Cobra Series Auto-Gamma Counter (Packard Instrument Co., Meriden,

CT) to determine surface bound A11. Lastly, the cells were solubilized by adding 1 mL of a 1 N NaOH solution to each dish for 30 min, followed by another 1 mL NaOH wash. The two NaOH washes were collected, and the radioactivity in the solution was quantified as described above to determine the amount of internalized A11. Each entire experiment was performed three times, where triplicate measurements were obtained for each time point in each experiment.

Making Polypeptide-Based Gold Nanoshells

The $K_{60}L_{20}$ block copolypeptide was synthesized by transition-metal-initiated α-amino acid *N*-carboxyanhydride polymerization as previously described[11]. After freeze-drying, the $K_{60}L_{20}$ polypeptide was processed into vesicles using a modification of a method previously reported[11-13]. Specifically, the vesicles were formed by first dissolving 10 mg of polypeptide in 1 mL of a 15% tetrahydrofuran (THF) solution in sterile Milli-Q water. Another 1 mL of a 15% THF solution was then added to yield a final polypeptide concentration of 0.5% w/v. Subsequently, the mixture was placed in a dialysis bag (MWCO = 8,000 Da) and dialyzed against sterile Milli-Q water overnight to remove the THF, where the sterile Milli-Q water was changed every hour for the first 4 hours. After processing, the $K_{60}L_{20}$ vesicles were serially extruded through polycarbonate membranes with 1000, 400, 200, and lastly 100 nm pores in order to obtain a uniform vesicle size. A 4.63 mL suspension of the resulting polypeptide vesicles (1.34 mg) was adjusted to pH 7 using 7% ammonium hydroxide (Sigma-Aldrich, St. Louis, MO). Hydroxylamine hydrochloride (Sigma-Aldrich, St. Louis, MO) was added in excess (500 µL of a 0.2 M solution), followed by 154 µL of a 0.5% gold (III) chloride solution (Sigma-Aldrich, St. Louis, MO) in two 77-µL aliquots. The suspension was allowed to spin overnight, and the gold-coated vesicles were recovered by centrifugation at 9,000 rcf for 10 min. The pH

was found to be critical in the gold-coating process; therefore, the pH was adjusted as needed to maintain a pH of 7 throughout the coating process.

Conjugation Scheme for A11 and PEG to Polypeptide-Based Gold Nanoshells

Gold nanoshells can be surface-functionalized with thiol-containing moieties through dative bonds. In order to conjugate A11 to the gold nanoshells, we cleaved the disulfide linker between the constant regions of the minibody to expose free thiols. Briefly, free thiol groups on A11 were exposed by breaking the disulfide linkages between the heavy chains using a 3:1 molar ratio of the minibody to dithiolthreitol (DTT), enabling conjugation to the gold nanoshells through dative bonds. The free DTT was then purified from the thiolated A11 using 10K MWCO spin concentrators (EMD Millipore, Billerica, MA). We also saturated the gold nanoshell surface using thiol-functionalized polyethylene glycol (PEG). To conjugate the PEG and A11 to the gold nanoshells, the pH of the gold nanoshell suspension was adjusted to 9 using 1.5 M NaOH. Monofunctional methoxy-PEG-thiol (5,000 MW) (Nanocs, Boston, MA) and thiolated A11 were added at a molar ratio of 10000:1000:1 PEG:A11:gold nanoshell. To ensure adequate conjugation of A11, 0.08 mg of A11 were added to the gold nanoshells first, and allowed to react for 30 min while stirring, followed by the conjugation of 0.1 mg PEG for 10 min. Free PEG and A11 were purified by centrifugation at 2000 rcf for 2 min. To provide stability during the recovery process, we added bovine serum albumin (BSA) in excess (50 µL of 10% w/v BSA) to passivate the surfaces of the plastic tube as well as the gold nanoshell. To make the PEGylated gold nanoshells, a similar protocol was followed without the addition of A11.

Characterization of A11-Conjugated Gold Nanoshells

Size measurements were performed on the A11-conjugated and PEGylated gold nanoshells with the Malvern Zetasizer Nano ZS model Zen 3600 (Malvern Instruments Inc., Westborough, MA). For the transmission electron microscopy (TEM), the colloidal gold nanoshells were first mixed by pipetting multiple times and immediately applied to carbon-coated copper grids. The grids were air-dried without staining or blotting. TEM images were then recorded inside an FEI T20 200kV transmission electron microscope on an FEI Eagle 4 megapixel CCD camera. The extinction profile of the gold nanoshells was measured to verify the significant surface plasmon resonance in the near infrared region using a UV-visible-NIR spectrophotometer (Thermo Scientific BioMate 3S) over a range of wavelengths from 400 to 1100 nm.

Measuring Heat Generation

Gold nanoshells (extinction at 808 nm = 0.2 a.u.) were irradiated with a 200 mW laser diode, 808 nm (ThorLabs, Inc., Newton, NJ) for 10 min at a power density of approximately 33 W cm^{-2}. The temperature was measured at desired time points using a thermocouple (OMEGA Engineering INC. Model HYP-0, Stamford, CT) placed into a 96 well plate in 100 μL of the gold nanoshell suspension in water.

Mathematical Model for Heat Transfer of A11 Minibody-Conjugated Gold Nanoshells

Our laboratory previously derived a detailed mathematical model for heat transfer from gold nanoshells[15]. This model was improved by relaxing a few of our previous assumptions.

The previous model assumed the rate of mass loss to evaporation was a constant. We relaxed this assumption, and allowed the rate of mass lost to evaporation to vary as a function of

temperature based on the mathematical relations reported by Saylor and coworkers[16]. Briefly, the mass transfer coefficient due to evaporation is defined in **Eq. (1)**:

$$h_m = \frac{\dot{m}''}{\Delta\rho_{wv}} \quad (1)$$

where h_m is the mass transfer coefficient (m s^{-1}), $\dot{m}''$ is the mass flux (kg m^{-2} s^{-1}), and $\Delta\rho_{wv}$ is defined in **Eq. (2)**:

$$\Delta\rho_{wv} = \rho_{wv,s} - \gamma\ \rho_{wv,a} \quad (2)$$

where $\rho_{wv,s}$ is the saturated vapor density at the water surface (kg m^{-3}), $\rho_{wv,a}$ is the saturated vapor density in ambient air (kg m^{-3}), and γ is the relative humidity immediately above the air-water interface, which was set to be 75% throughout the experiment. To evaluate both saturated vapor densities, the saturated vapor pressures at the appropriate temperatures were first determined using the Antoine equation, followed by a conversion from saturated vapor pressure to density using the ideal gas equation of state. The Sherwood number (Sh), which is defined as the ratio of the convective mass transfer to the rate of diffusive mass transport alone, is given by **Eq. (3)**:

$$Sh = \frac{W\ h_m}{D} \quad (3)$$

where W is the diameter of the well (m), and D is the diffusion coefficient of water vapor in air (m^2 s^{-1}), which was also modeled as a function of temperature[17]. The Sherwood number was correlated to the Rayleigh number (Ra), which is the product between the ratio of buoyancy to viscous forces and the ratio of momentum to thermal diffusivities[18]:

$$Sh = (0.0019)Ra^{0.329} \quad (4)$$

The Rayleigh number (Ra) is defined as follows[16]:

$$Ra = \frac{g\ \Delta\rho\ W^3}{\bar{\rho}\ \upsilon\ \alpha} \quad (5)$$

where g is the acceleration due to gravity at sea level (m s^{-2}), Δρ is the difference between the air/vapor mixture densities at the water surface and at ambient air (kg m^{-3}), and $\bar{\rho}$ is the average air/vapor mixture density between the water surface and ambient air (kg m^{-3}). To determine both densities, the average air/vapor mixture pressures at the appropriate temperatures were first determined with the Antoine equation, followed by converting the average air/vapor mixture pressures to densities using the ideal gas equation of state. In addition, υ and α are the kinematic viscosity (m^2 s^{-1}) and the thermal diffusivity (m^2 s^{-1}) of air, respectively. Both υ and α were also modeled as a function of temperature based on the correlations provided by Tsilingiris[19]. Thus, by using **Eq. (2)-(5)**, the rate of mass loss to evaporation (kg s^{-1}) can be calculated as a function of temperature.

Furthermore, the convective heat transfer coefficient of air was also modified from our previous model to better reflect the experimental conditions. The Nusselt-Rayleigh correlation that was incorporated in our new version of the model is given by **Eq. (6)**[20]:

$$Nu = (1.759)\, Ra^{0.130} \qquad (6)$$

where[16]:

$$U_{air} = \frac{Nu\ \lambda_{air}}{W} \qquad (7)$$

and U_{air} is the convective heat transfer coefficient of air (W m^{-2} K^{-1}), and λ_{air} is the thermal conductivity of air (W m^{-1} K^{-1}), which was modeled as a function of temperature based on the correlations provided by Tsilingiris[19], Using **Eqs. (5)-(7)**, U_{air} can also be calculated as a function of temperature. Note that our previous model had used constants for parameters in the Nu equation (**Eq. (7)**), while we are now allowing these parameters to vary with temperature. All of the other model components were the same as those previously reported[15].

Photothermal Therapy Using A11-Conjugated Gold Nanoshells

Gold nanoshells were incubated with PSCA-expressing 22Rv1 prostate cancer cells for 30 min in serum-free media. After incubation, cells were washed with PBS. 100 µL of PBS were then added to the wells, and the cells were irradiated with an 808 nm laser diode at a power density of approximately 33 mW/cm^2 for 10 min. A Live/Dead Stain Kit (calcein AM and ethidium homodimer, Molecular Probes, CA, USA) was used to evaluate the viability of the cells. Cells were examined using fluorescent microscopy with an EVOS fl Digital Inverted Fluorescence Microscope (Advanced Microscopy Group/Life Technologies, Grand Island, NY).

3. Results

Determining the internalization rate constant of the A11 Minibody

In order to determine the internalization rate constant of the A11 minibody, a model of the cellular trafficking pathway was developed based on a species balance on the internalized A11-antigen complexes. The change in internalized complexes with respect to time can be increased through internalization of the surface-bound complexes and decreased through both recycling and degradation of the internalized complexes (**Eq. (8)**):

$$\frac{dC_i}{dt} = k_{int}C_s - k_{rec}C_i - k_{deg}C_i \qquad (8)$$

where C_i is the concentration of internalized A11-antigen complexes, t is the time, k_{int} is the internalization rate constant, C_s is the concentration of surface-bound A11, k_{rec} is the recycling rate constant, and k_{deg} is the degradation rate constant.

Short time points (less than 10 min) were chosen so that recycling and degradation were negligible in the experiment. Integrating the resulting equation using the initial condition that no A11 is present inside the cell yields **Eq. (9)**:

$$C_i = k_{int} \int_0^t C_s \, dt' \quad (9)$$

Based on **Eq. (9)**, the internalization rate constant can be determined as the slope of the graph of the concentration of internalized A11 as a function of the integral of the concentration of surface complexes over time. To obtain this data, radiolabeled A11 was incubated with PSCA-expressing 22Rv1 prostate cancer cells, and the surface-bound and internalized radiolabeled A11 were quantified at the desired time points. The trapezoidal rule was then applied to obtain the integral of the surface complexes over time. Plotting the data based on the math model (**Eq. (9)**), the internalization rate constant was determined as the slope of the plot of the internalized A11 as a function of the integral of the cell-surface complexes over time. The average internalization rate constant for PSCA-expressing 22Rv1 cells was found to be 0.0073 min^{-1} (**Figure 1**).

A11 Minibody-Conjugated Polypeptide-Based Gold Nanoshells

Dynamic light scattering characterization of the A11 minibody and polyethylene glycol (PEG)-conjugated gold nanoshells and the PEGylated gold nanoshells without A11 showed that both types of nanoshells were around 200 nm in size with polydispersity indices being 0.14 and 0.21, respectively (**Table 1)**. Direct observation of these nanoshell preparations under TEM confirmed these dynamic light scattering results, revealing spherical gold particles with various diameters up to 200 nm (**Figure 2**). Furthermore, the extinction profiles demonstrated that the targeted and non-targeted gold nanoshells maintained strong surface plasmon resonance in the near infrared region (**Figure 3**).

Mathematical Model for Heat Transfer of A11 Minibody-Conjugated Gold Nanoshells

To gain a better understanding of our A11 minibody-conjugated gold nanoshells in the context of photothermal therapy. We improved the mathematical model for heat transfer that was previously developed by our research group for heat generation of gold nanoshells[15]. The mathematical model was solved numerically using finite difference equations and the method of lines, which were coded into the MATLAB programming language. The temperature increase as a function of time for the gold nanoshells was predicted using the mathematical model, and the prediction was compared with our experimental measurements of temperature. Our revised model was able to reasonably predict the rise of the temperature, especially near the beginning of the experiment (**Figure 4**). It is important to include the temperature dependence of the parameters affecting the evaporation rate and the heat transfer coefficient as the temperatures are relatively lower at the beginning of the heat generation experiment.

PSCA-Targeted Photothermal Therapy Using Polypeptide-Based Gold Nanoshells

As shown in **Figure 5**, both the targeted and non-targeted gold nanoshells generated significant amounts of heat within 10 min and with similar heating profiles. Using these gold nanoshells *in vitro*, we demonstrated localized and specific laser-induced cytotoxicity, where PSCA-expressing 22Rv1 cells incubated with targeted gold nanoshells showed cell death only within the laser-irradiated region (**Figure 6 a, b**). No similar region was observed for the non-targeted gold nanoshells (**Figure 6 c, d**).

4. Discussion

This work represents the first successful development of an A11 minibody-conjugated near infrared-responsive gold nanoshell for photothermal therapeutic treatment of prostate cancer. Before developing the gold nanoshells, we first characterized the internalization rate constant of A11 to quantitatively confirm observations that A11 does not significantly internalize into prostate cancer cells. Using an ordinary differential equation for the number of internalized A11-PSCA complexes and performing radiolabeling experiments, the internalization rate constant was determined for PSCA-transfected 22Rv1 prostate cancer cells. Similar to previous reports[5], we observed rapid binding of A11 to PSCA-expressing cells; however, cellular internalization was relatively low. We chose to focus on the binding and internalization processes at short time points (less than 10 min), where degradation and recycling processes could be neglected, thereby allowing us to focus on the binding and internalization processes. The average internalization rate constant for PSCA-expressing 22Rv1 cells was found to be considerably less than the internalization rate constant for ligands known to be endocytosed by

cells. For example, the internalization rate constant of transferrin in HeLa cells is about 0.38 min^{-1} [21], while that of epidermal growth factor in A431 epidermoid carcinoma cells is between 0.04 to 0.16 min^{-1} [22]. In addition, the internalization rate constant of insulin in Chinese Hamster Ovary cells is approximately 0.187 min^{-1} [23], while that of vascular endothelial growth factor in human umbilical vein endothelial cells is approximately 0.282 min^{-1} [24]. Based on the internalization properties of the A11 minibody, we chose to develop a nanoparticle system that could exert its toxic effect while remaining bound to the surface of the cell.

Here, we combined the prostate cancer-targeting ligand, the A11 minibody, with our novel polypeptide-based gold nanoshells for use as a photothermal therapy agent. We characterized their size and morphology using dynamic light scattering and transmission electron microscopy, investigated the ability to generate heat upon laser irradiation, and evaluated the enhanced efficacy for treatment of PSCA-expressing prostate cancer cells.

To create the gold nanoshells, we reduced gold onto the surface of the $K_{60}L_{20}$ vesicles. Next, to provide *in vivo* stability, we conjugated PEG to the surface through dative bonds, where PEG has been demonstrated to prevent aggregation and nonspecific adsorption of serum proteins. Characterization of the gold nanoshells after conjugation showed that the particles were relatively monodisperse and within the size range for passive targeting of solid tumors, such as prostate cancer tumors. Passive targeting, which is possible due to the enhanced permeability and retention effect of solid tumors, has been demonstrated for particles within the size range of 60-400 nm in diameter due to the leaky vasculature and poor lymphatic drainage at the tumor site[25]. Additionally, the extinction profile of the gold nanoshells indicated that they would be responsive to near infrared irradiation.

The photothermal therapeutic properties of the gold nanoshells *in vitro* were also investigated. To evaluate their ability to generate heat in response to near infrared irradiation, we measured the temperature as a function of exposure time to 808 nm, narrow band illumination. The water surrounding the gold nanoshells demonstrated an 18 degree Kelvin increase in temperature over the 10-min experiment, which was also supported by our mathematical model. Our updated parameters improved our prediction of the initial temperature rise of our gold nanoshells upon near-infrared irradiation. Furthermore, the targeted and non-targeted gold nanoshells showed similar heating profiles. To determine if the temperature increase could cause cellular toxicity, we incubated the targeted and non-targeted gold nanoshells in the presence of PSCA-expressing prostate cancer cells. Upon laser irradiation, significant and localized cell death occurred within the irradiated region for the A11-conjugated gold nanoshells, while little to no cell death was observed for the non-targeted gold nanoshells. These results indicate that the A11 minibody enhances the cellular binding and association of gold nanoshells, which results in greater efficacy of the therapy.

In conclusion, we have demonstrated the ability to create A11-conjugated gold nanoshells with the appropriate size and heat generation properties for photothermal treatment of prostate cancer. The PSCA-targeted polypeptide-based gold nanoshells also showed promise by exhibiting greater efficacy as a photothermal therapy agent compared to non-targeted gold nanoshells.

Acknowledgments

This work was supported by a grant from the National Science Foundation (DMR 1308081) to T.J.D. and D.T.K., as well as the National Science Foundation Graduate Research Fellowship (DGE-1144087) to K.M.M. We also acknowledge the use of instruments in the Electron Imaging Center for Nanomachines core facility supported by NIH (1S10RR23057 and GM071940 to Z.H.Z.) and CNSI at UCLA.

References

1 Reiter, R. E.; Gu, Z.; Watabe, T.; et al. Prostate Stem Cell Antigen: A Cell Surface Marker Overexpressed in Prostate Cancer. *Proc. Natl. Acad. Sci.* **1998**, 95, 1735–1740.

2 Gu, Z.; Thomas, G.; Yamashiro, J.; et al. Prostate Stem Cell Antigen (PSCA) Expression Increases with High Gleason Score, Advanced Stage and Bone Metastasis in Prostate Cancer. *Oncogene*. **2000**, 19, 1288–1296.

3 Lepin, E. J.; Leyton, J. V.; Zhou, Yu.; et al. An Affinity Matured Minibody for PET Imaging of Prostate Stem Cell Antigen (PSCA) - Expressing Tumors. *Eur. J. Nucl. Med. Mol. Imaging*. **2010**, 37, 1529–1538.

4 Gagnon, P.; Cheung, C. W.; Lepin, E. J.; et al. Minibodies and Multimodal Chromatography Methods: A Convergence of Challenge and Opportunity. *Bioprocess Int.* **2010***,* 8, 26-35.

5 Knowles, S. M.; Zettlitz, K. A.; Tavare, R.; et al. Quantitative ImmunoPET of Prostate Cancer Xenografts with ^{89}Zr- and ^{124}I-Labeled Anti-PSCA A11 Minobody. *J. Nucl. Med.* **2014**, 55, 452–459.

6 Kelly, K. L.; Coronado, E.; Zhao, L. L.; & et al. The Optical Properties of Metal Nanoparticles: The Influence of Size, Shape and Dielectric Environment. *J. Phys. Chem. B*. **2003**, 107, 668–677.

7 Wang, S.; Riahi, R.; Li, N.; et al. Single Cell Nanobiosensors for Dynamic Gene Expression Profiling in Native Tissue Microenvironments. *Adv. Mater.* **2015**, 27, 6034–6038.

8 Riahi, R.; Wang, S.; Long, M.; et al. Mapping Photothermally Induced Gene Expression in Living Cells and Tissues by Nanorod-Locked Nucleic Acid Complexes. *ACS Nano.* **2014**, 8, 3597–3605.

9 Qin, Z.; Bischof, J. C.; Thermophysical and Biological Responses of Gold Nanoparticles Laser Heating. *Chem. Soc. Rev.* **2012**, 41, 1191–1217.

10 Tong, L.; Zhao, Y.; Huff, T. B.; et al. Gold Nanorods Mediate Tumor Cell Death by Compromising Membrane Integrity. *Adv. Mater.* **2007**, 19, 3136-3141.

11 Holowka, E. P.; Pochan, D. J.; Deming, T. J.; Charged Polypeptide Vesicles with Controllable Diameter. *J. Am. Chem. Soc.* **2005**, 127, 12423–12428.

12 Sun, V. Z.; Choe, U. J.; Rodriguez A. R.; et al. Transfection of Mammalian Cells Using Block Copolypeptide Vesicles. *Macromol. Biosci.* **2013**, 13, 539–550.

13 Holowka, E. P.; Sun, V. Z.; Kamei, D. T.; et al. Polyarginine Segments in Block Copolypeptides Drive Both Vesicular Assembly and Intracellular Delivery. *Nat. Mater.* **2007**, 6, 52–57.

14 Lake-Bakaar, G.; Rubio, C. E.; Mckavanagh, S.; et al. Metabolism of ^{125}I-Labelled Trypsin in Man: Evidence of Recirculation. *Gut*. **1980**, 21, 580–586.

15 Mayle, K. M.; Dern, K. R.; Wong, V. K.; et al. Polypeptide-Based Gold Nanoshells for Photothermal Therapy. *J. Lab. Autom.*, **2016**

16 Bower, S. M.; Saylor, J. R.; A Study of the Sherwood-Rayleigh Relation for Water Undergoing Natural Convection-driven Evaporation. *Int. J. Heat Mass Tran.* **2009**, 52, 3055-3063.

17 Gates, D. M. Biophysical Ecology; Springer Verlag: New York, **1980**.

18 Bower, S. M.; Saylor, J. R.; International Mechanical Engineering Congress and Exposition. Seattle, WA, November 11-15, **2007**; The American Society of Mechanical Engineers.

19 Tsilingiris, P. T.; Thermophysical and Transport Properties of Humid Air at Temperature Range Between 0 and 100℃. *Energ. Convers. Manage.* **2008**, 49, 1098-1110.

20 Kobus, C. J.; Wedekind, G. L.; An Experimental Investigation into Natural Convection Heat Transfer from Horizontal Isothermal Circular Disks. *Int. J. Heat Mass Tran.* **2001**, 44, 3381-3384.

21 Yazdi, P. T.; Murphy, R. M.; Quantitative Analysis of Protein Synthesis Inhibition by Transferrin-Toxin Conjugates. *Cancer Res.* **1994**, 54, 6387–6394.

22 Wiley, H. S.; Anomalous Binding of Epidermal Growth Factor to A431 Cells is Due to the Effect of High Receptor Densities and a Saturable Endocytic System. *J. Cell Biol.* **1988**, 107, 801–810.

23 Backer, J. M.; Shoelson, S. E.; Haring, E.; et al. Insulin Receptors Internalize by a Rapid, Saturable Pathway Requiring Receptor Autophosphorylation and An Intact Juxtamembrane Region. *J. Cell Biol.* **1991**, 115, 1535-1545.

24 Anderson, S. M.; Shergill, B.; Barry, Z. T.; et al. VEGF Internalization Is Not Required For VEGFR-2 Phosphorylation in Bioengineered Surfaces with Covalently Linked VEGF. *Integr. Biol. (Camb).* **2011**, 3, 887-896.

25 Maeda, H.; Wu, J.; Sawa, T.; et al. Tumor Vascular Permeability and the EPR Effect in Macromolecular Therapeutics: A Review. *J. Control. Release*. **2000**, 65, 271–284.

Table 1. Characterization of A11 minibody-conjugated and PEGylated polypeptide-based gold nanoshells and PEGylated polypeptide-based gold nanoshells without the A11 minibody. The range of values correspond to standard deviations from 3 measurements of the sample.

$K_{60}L_{20}$ Vesicles	Size (nm)	Polydispersity Index (PDI)
Gold-coated	148 ± 3	0.11 ± 0.01
PEGylated and Gold-coated	183 ± 4	0.14 ± 0.03
A11 Minibody-conjugated, PEGylated, and Gold-coated	200 ± 5	0.21 ± 0.01

Figure Legends

Figure 1. Determining the A11 internalization rate constant for PSCA-transfected 22Rv1 prostate cancer cells. The entire experiment was performed three times, and the error bars correspond to standard deviations.

Figure 2. TEM images of (**a**) A11 minibody-conjugated and PEGylated polypeptide-based gold nanoshells and (**b**) PEGylated polypeptide-based gold nanoshells without the A11 minibody. Scale bar is 200 nm.

Figure 3. Extinction profiles of (**a**) A11 minibody-conjugated and PEGylated polypeptide-based gold nanoshells and (b) PEGylated polypeptide-based gold nanoshells without the A11 minibody.

Figure 4. Comparison of our mathematical model predictions (orange circle) with our measured temperatures (blue circle) for A11 minibody-conjugated and PEGylated gold nanoshells in water

with exposure to an 808-nm laser diode (200mW). The error bars on the experimental data correspond to standard deviations from triplicate measurements.

Figure 5. Heat generation as a function of time for targeted (blue diamonds) and non-targeted (red squares) PEGylated polypeptide-based gold nanoshells. Error bars correspond to standard deviations from triplicate measurements.

Figure 6. Laser-induced cytotoxicity for (**a, b**) targeted A11-conjugated and PEGylated gold nanoshells and (**c, d**) non-targeted PEGylated gold nanoshells. Live cells are shown in green (calcein AM stain) and dead cells are shown in red (ethidium homodimer stain). Scale bar = 1 mm. (Extinction at 808 nm = 0.4 a.u.).

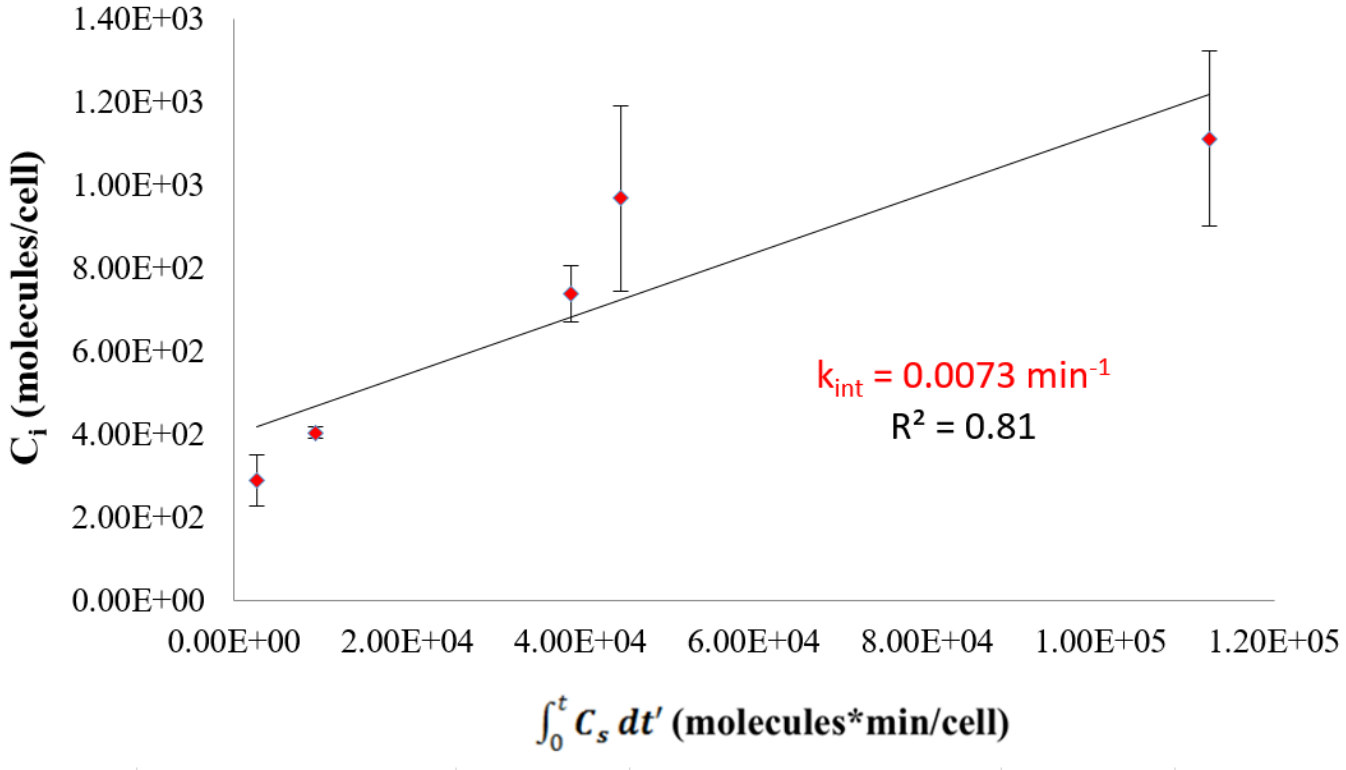

Figure 1. Determining the A11 internalization rate constant for PSCA-transfected 22Rv1 prostate cancer cells. The entire experiment was performed three times, and the error bars correspond to standard deviations.

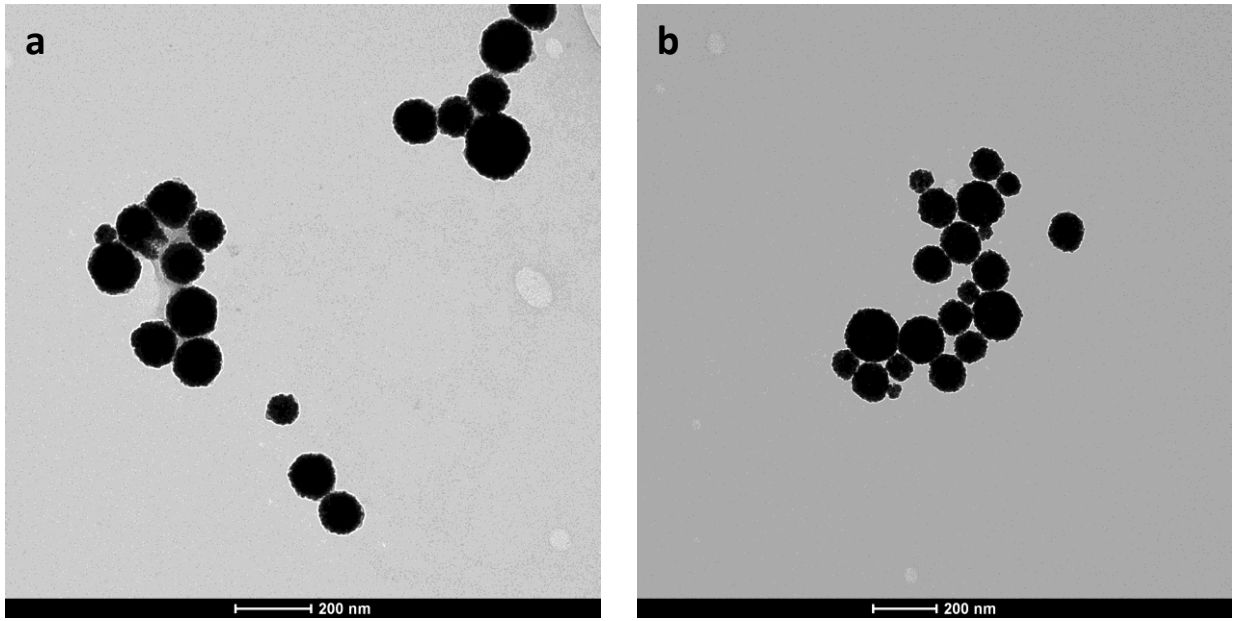

Figure 2. TEM images of (**a**) A11 minibody-conjugated and PEGylated polypeptide-based gold nanoshells and (**b**) PEGylated polypeptide-based gold nanoshells without the A11 minibody. Scale bar is 200 nm.

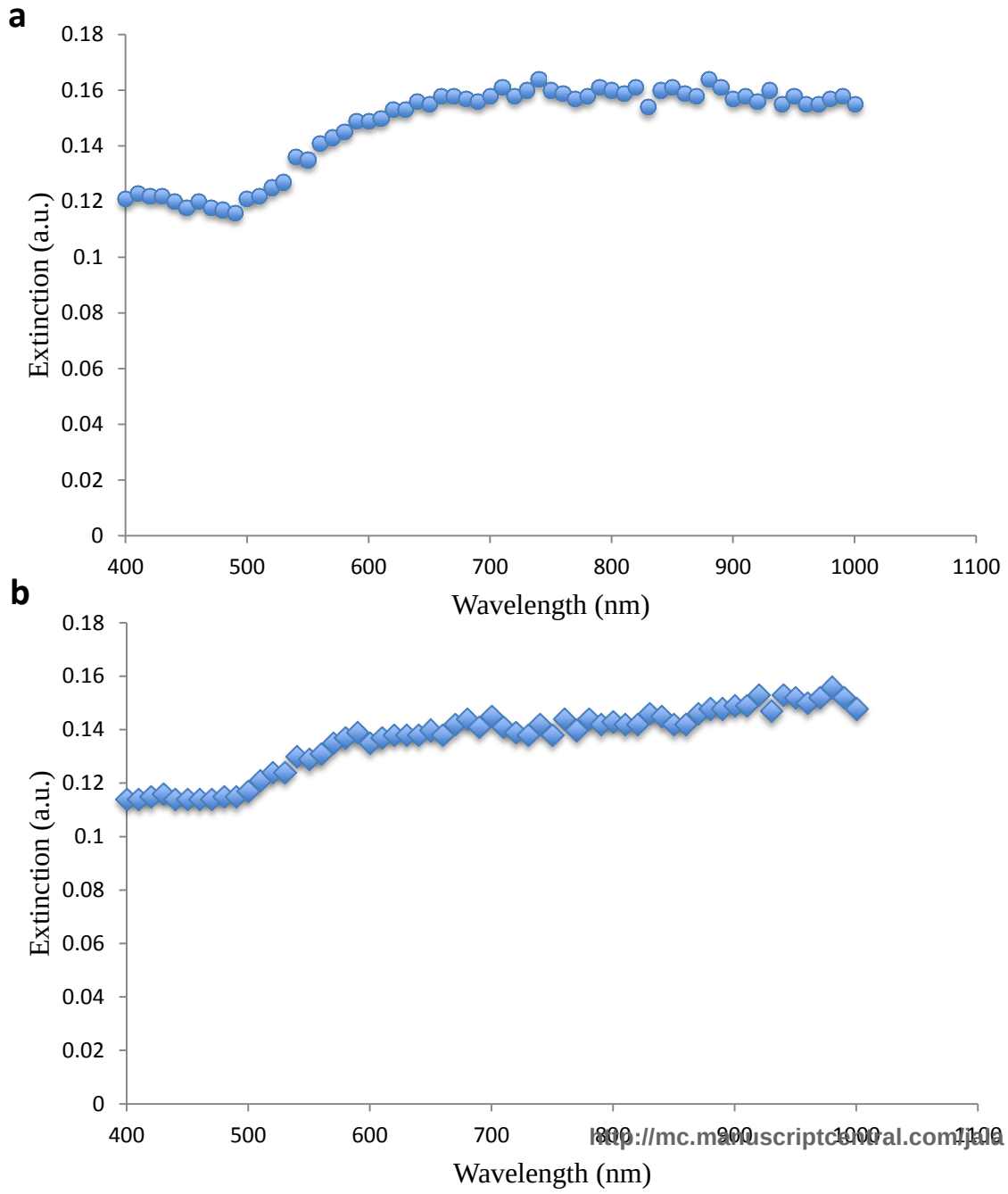

Figure 3. Extinction profiles of (**a**) A11 minibody-conjugated and PEGylated polypeptide-based gold nanoshells and (b) PEGylated polypeptide-based gold nanoshells without the A11 minibody.

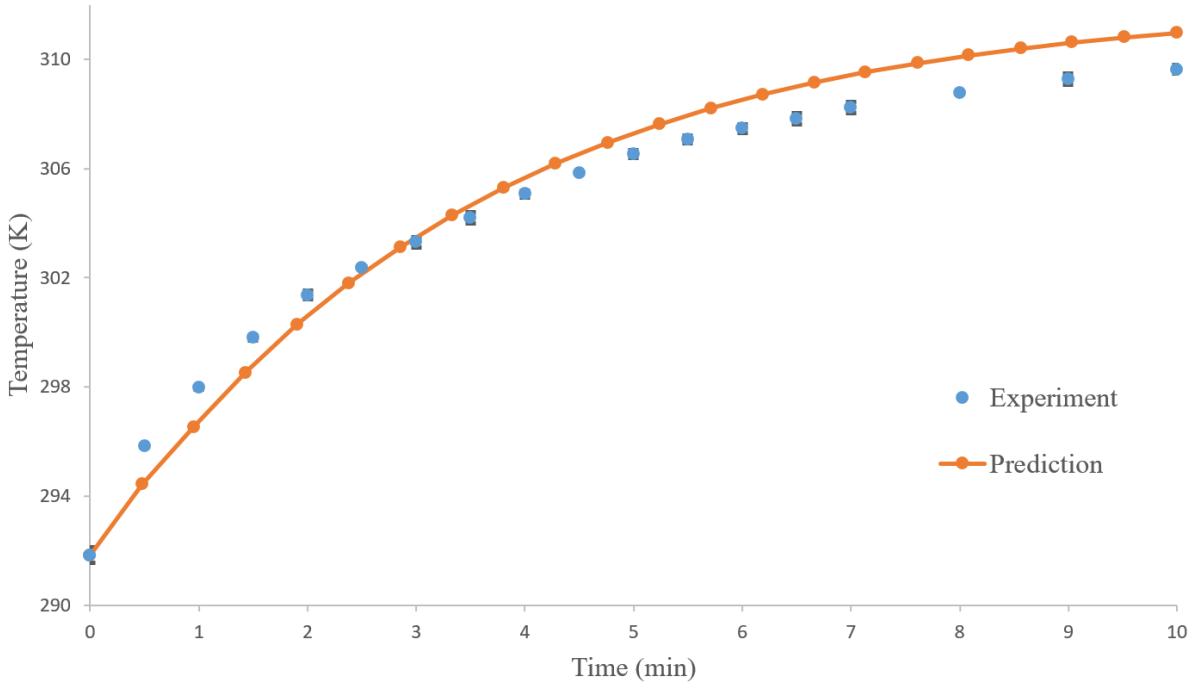

Figure 4. Comparison of our mathematical model predictions (orange circle) with our measured temperatures (blue circle) for A11 minibody-conjugated and PEGylated gold nanoshells in water with exposure to an 808-nm laser diode (200mW). The error bars on the experimental data correspond to standard deviations from triplicate measurements.

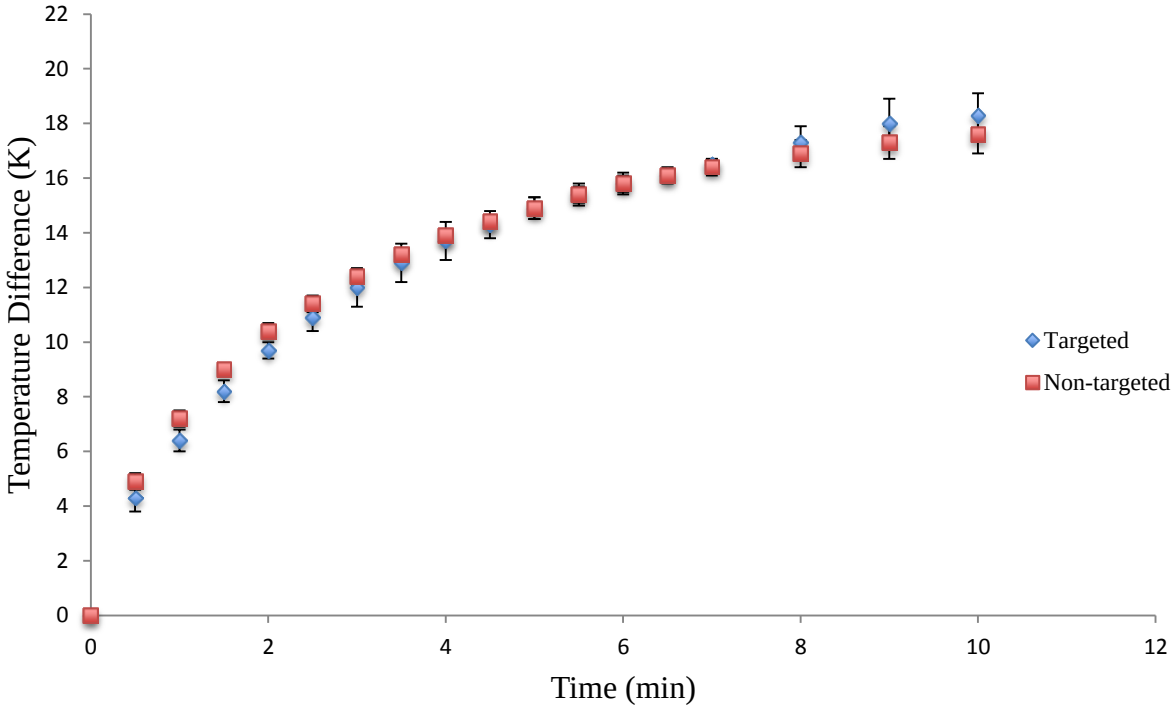

Figure 5. Heat generation as a function of time for targeted (blue diamonds) and non-targeted (red squares) PEGylated polypeptide-based gold nanoshells. Error bars correspond to standard deviations from triplicate measurements.

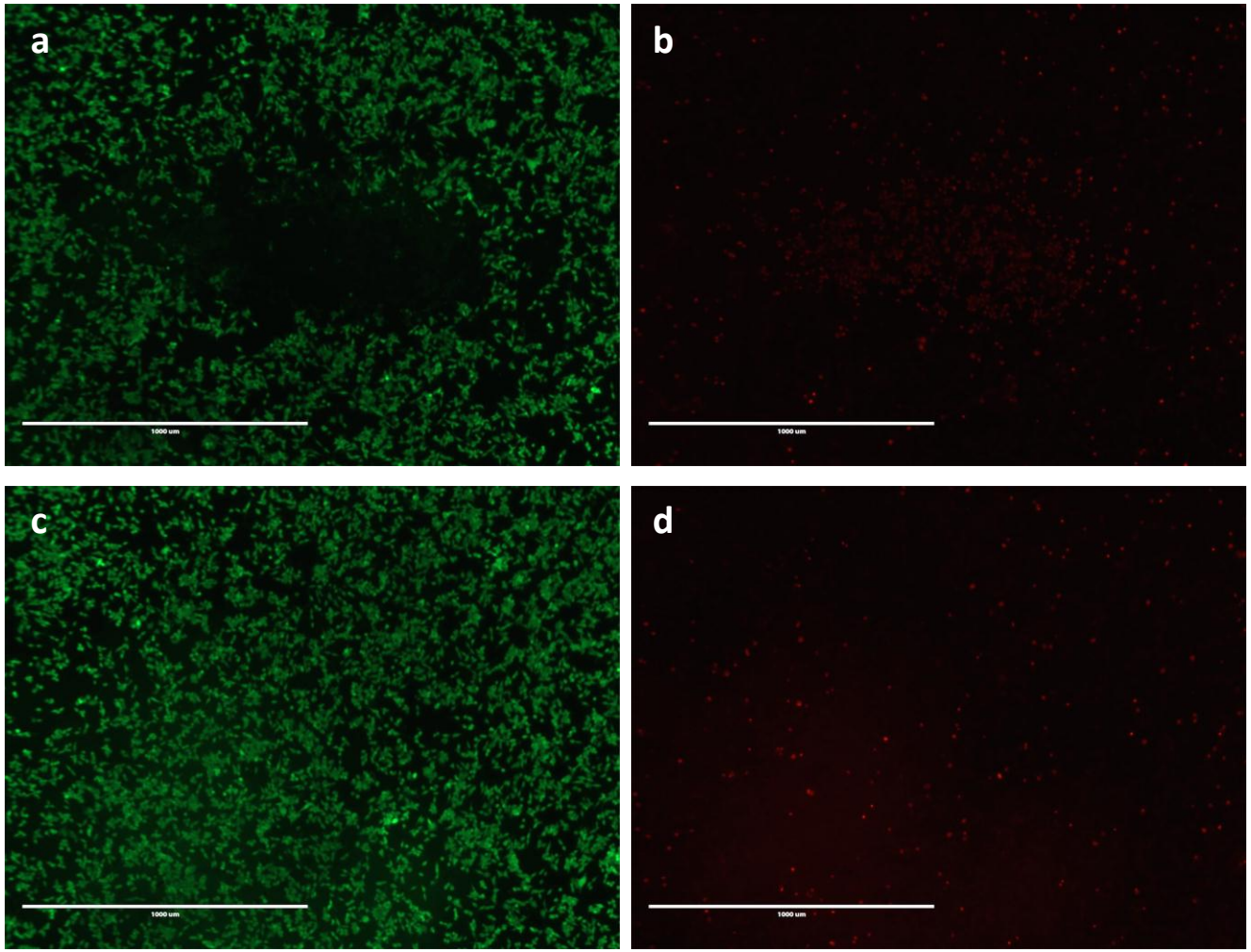

Figure 6. Laser-induced cytotoxicity for (**a, b**) targeted A11-conjugated and PEGylated gold nanoshells and (**c, d**) non-targeted PEGylated gold nanoshells. Live cells are shown in green (calcein AM stain) and dead cells are shown in red (ethidium homodimer stain). Scale bar = 1 mm. (Extinction at 808 nm = 0.4 a.u.).